

Effect of annealing temperature on the structural and optical properties of ZnSe nanoparticles

Kanta Yadav · Y. Dwivedi · Neena Jaggi

Received: 14 October 2014 / Accepted: 3 January 2015 / Published online: 10 January 2015
© Springer Science+Business Media New York 2015

Abstract In the present study, zinc selenide (ZnSe) nanoparticles (NPs) were synthesized by hydrothermal method and effect of annealing at different temperatures (100, 300, 500 and 700 °C) was monitored using various characterization techniques. It was observed and confirmed that ZnSe NPs oxidized on annealing at high temperature 700 °C and more than 70 % of ZnSe converted into ZnO NPs. The prepared NPs were characterized by X-ray diffraction and field emission scanning electron microscope, while spectroscopic characterizations were done by UV–Visible absorption, Photoluminescence (PL) emission, Raman scattering and Photoluminescence excitation (PLE) techniques. PL and PLE spectra confirmed strong interaction between the synthesized NPs, through the process of energy transfer, which resulted in bright blue–green colour emission of ZnSe and defect emissions of ZnO NPs.

1 Introduction

Now-a-days in materials science a great interest of research is focused on to control crystal intensification with desired quality, shape and size. Recently nanoparticles (NPs) have gained more significance due to increased surface area which is required to enhance the efficiency of both optical and electronic devices. The group II–VI semiconductor nanocrystals (NCs) have smaller radii than the bulk exciton Bohr radius, giving a new class of materials whose

properties are amid molecular and bulk materials. Semiconductor NPs having sizes smaller than or equal to the Bohr diameter of the exciton, give rise to quantum confinement effects leading to increased energy band gaps and discrete energy levels [1]. Most II–VI semiconductors show quantum confinement behavior below 20 nm, and show different optical, electronic and mechanical properties from those of their bulk counterparts. Quantum confinement of both electron and hole in all proportions lead to enhancement in the band gap with decrease in size of NCs [2]. Also the effect of temperature on the structural properties of the group II–VI semiconductor NPs has been a field of ongoing research with regard to their phase transformation or complete oxidation to another compound. Venkatachalam et al. [3] reported that the particle size increases whereas strain and dislocation density decrease with increase of substrate temperature. Ndiaye et al. [4] have reported on transition of CdSe thin films from amorphous (cubic) to hexagonal after CdCl₂ treatment at 723 K. Sivasubramanian et al. [5] have reported the phase transformation from cubic to hexagonal upon annealing the CdS NPs. Amaranatha Reddy et al. [6] have confirmed that after annealing at 500 °C cubic ZnS NPs converted to wurtzite ZnO NPs.

Zinc Selenide (ZnSe) is an important group II–VI n type semiconductor material with intrinsic direct energy band gap ($E_g = 2.7$ eV) and Bohr exciton diameter 9 nm [7–9]. The synthesis process of nanocrystalline ZnSe particles has a large impact on the phase, morphology and size of the NPs which in turn alter their physical and chemical properties [10]. Due to wide band gap, high luminescence efficiency and low absorption coefficient; ZnSe finds a great importance for short-wavelength lasers and other optoelectronic applications in light emitting diodes, photo- and electro- luminescent devices, quantum wells, sensors

K. Yadav · Y. Dwivedi · N. Jaggi (✉)
Department of Physics, National Institute of Technology,
Kurukshetra 136 119, Haryana, India
e-mail: neena_jaggi@rediffmail.com

K. Yadav
e-mail: kantayad@gmail.com

and thin film solar cells [11–13]. The intense emission spectra, continuous absorption band, high chemical and photo bleaching constancy, and exterior functionality are among the most attractive properties of ZnSe NPs, which are not available from either bulk material or isolated atoms [14].

ZnSe NPs have been synthesized by different techniques: sol gel, aqueous chemical, chemical deposition, microemulsion, chemical precipitation and hydrothermal [15–19]. The surface alteration of the grown NCs has been done to avoid self agglomeration of particles leading to size control and uniform size distribution of particles. The hydrothermal approach utilized in the present study is a simple and economical method, which is effective to control the particle size and uniform production of ZnSe NPs. The purity of sample synthesized by hydrothermal route is much better than the purity of the starting raw materials due to self-purifying property of the hydrothermal crystallization, as impurities present in the medium are eliminated by the growing crystallites [20, 21].

The objective of the present study is to prepare ZnSe NPs using hydrothermal method and monitor the effect of annealing temperature (100, 300, 500 and 700 °C) on structural and optical properties of ZnSe NPs. The studies revealed that ZnSe NPs having cubical symmetry are reduced to ZnO NPs of wurtzite structure at temperature 500 °C or above. A strong interaction for the conversion of ZnSe NPs to ZnO NPs is also reported on the basis of possible energy transfer mechanism.

2 Experimental

2.1 Chemicals

For the synthesis of ZnSe NPs, the chemicals used were Zinc acetate [$\text{Zn}(\text{CH}_3\text{COO})_2 \cdot 2\text{H}_2\text{O}$] of purity $\geq 99\%$, elemental Selenium (Se) of purity 99%, Ethylene glycol ($\text{C}_2\text{H}_6\text{O}_2$) of purity 99% and Hydrazine hydrate [$(\text{N}_2\text{H}_4) \cdot \text{H}_2\text{O}$] of purity 80%. These chemicals were procured from Loba Chemie and used as such without further purification.

2.2 Synthesis

ZnSe NPs have been synthesized by hydrothermal route. Freshly prepared aqueous solutions of Zinc acetate, and elemental selenium were used as reactant materials. Initially, 10.97 gm Zinc acetate was dissolved in 100 ml of de-ionized water to prepare solution and stirred at 70 °C for 30 min. Another 2.36 gm elemental selenium was dissolved in 40 ml hydrazine hydrate and 20 ml ethylene glycol whilst stirring at 70 °C for 30 min. Solution thus prepared was transferred into aqueous Zinc acetate solution

and stirred for 2 h at 70 °C and pH value was maintained at 6. After the completion of reaction, the solution was poured to autoclave (stainless steel Teflon) and kept at 100 °C for 15 h and allowed to cool at room temperature. This solution from the autoclave was filtered and precipitates were washed with ethanol and distilled water. The wet precipitates were dried in an oven at 100 °C for 5 h. The powder sample thus obtained was annealed at different temperatures 300, 500 and 700 °C in a furnace for 3 h.

2.3 Characterization techniques

The crystal structure and phase identity of the synthesized samples were carried out by recording X-ray diffraction patterns on a Rigaku mini desktop diffractometer using graphite filtered Cu-K_α radiation ($\lambda = 1.54 \text{ \AA}$) at 40 kV and 100 mA with a scanning rate of $3^\circ/\text{min}$ ($2\theta = 20\text{--}80^\circ$). UV–Visible absorption spectra were recorded on UV–Visible double beam 550 Spectrophotometer (Camspec) in the spectral range 200–800 nm using a spectral bandwidth of 1 nm at room temperature. Photoluminescence spectra of prepared samples were carried out on Shimadzu RF-530 Spectrofluorometer in the wavelength range 200–900 nm. The Raman spectra were recorded using 514.5 nm emission line of Ar^+ ion laser as the excitation wavelength on Renishaw micro-Raman set up at room temperature. Field emission scanning electron microscope image was carried out on a scanning electron micro-analyzer using a JEOL JSM-6700 microscope, operating at 10 A and 15 kV. The quantitative elemental composition analysis was carried out by energy dispersive X-ray (EDX) spectroscopy system attached with SEM of OXFORD analytical.

3 Results and discussion

3.1 X-ray diffraction analysis

The X-ray diffraction patterns of nanocrystalline ZnSe powder samples annealed at four temperatures viz 100, 300, 500 and 700 °C are shown in Fig. 1. The XRD spectra of the samples at 100 and 300 °C were found to be of cubical symmetry with three major Bragg-reflection peaks corresponding to three crystallographic planes (111), (220) and (311). These observed peaks are well consistent with those mentioned in the standard JCPDS No. 80-0021 (Fig. 1). On comparing the XRD patterns of the samples annealed at 100 and 300 °C, a shift of 0.2° towards higher angle in all the three peaks is observed giving rise to decrease in the interplaner spacing and lattice parameter indicating more alignment of atoms with lesser defect sites. Also the intensity of the peaks at 300 °C is increased depicting more crystalline behavior of ZnSe NPs at 300 °C

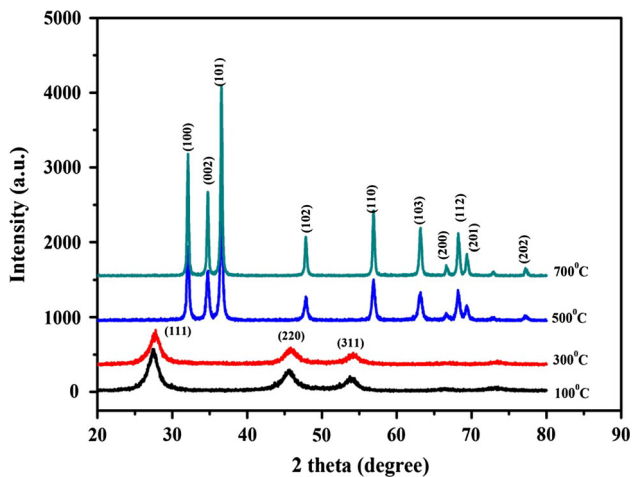


Fig. 1 XRD pattern of ZnSe sample annealed at different temperatures

as shown in Table 1. The crystallite size was calculated from the full-width at half maximum (FWHM) of diffraction peaks using the Debye–Scherrer expression

$$D_{hkl} = 0.9\lambda / (\beta_{hkl} \cos \theta) \quad (1)$$

where, D_{hkl} is the average crystalline diameter, λ is the wavelength in angstrom, β is full width at half-maximum and θ is the Bragg angle. The calculated values of crystallite sizes are 4.2 and 5.5 nm for samples annealed at 100 and 300 °C respectively as shown in Table 1.

On further annealing of ZnSe sample at 500 °C, XRD pattern showed a drastic change in the peaks location as compared to those for samples annealed at 100 and 300 °C depicting a change in the phase or altogether new structure formation. These observed peaks did not match with the other possible wurtzite phase of ZnSe NPs ruling out phase transformation. However, these peaks were matched to JCPDS No. 75-0576 corresponding to hexagonal structure of ZnO. This revealed that the prepared samples of ZnSe converted into ZnO at 500 °C since no diffraction peaks corresponding to any of ZnSe phase were found in the spectra. Such a phase conversion may occur under thermal stimulation which evokes atomic reconfiguration [22]. The intensity of the peaks sharply increased when phase conversion from ZnSe (cubic) to ZnO (hexagonal) took place. As the sample was further annealed at 700 °C the position of the diffraction peaks corresponding to ZnO remained invariant, however, there was an increment in the intensity of the peaks. Crystallite sizes were estimated using Eq. (1) and found to be 18.0 and 28.0 nm for samples annealed at 500 and 700 °C respectively as shown in Table 1. This enhancement in the intensity of the peak and crystallite size showed the improvement in the crystallinity of transformed ZnO NPs.

The crystallite size and strain have been calculated and graphically plotted with annealing temperature as shown in

Fig. 2. The crystallite size and strain are inversely proportional to each other with annealing temperature. The packing fraction of the prepared NPs is also calculated from the volume of atoms and cell (Table 1) and is 74 % in each case corresponding to highest packed solid materials.

3.2 Raman analysis

Raman spectroscopy is one of the most widely used techniques to investigate the phase formation and structure of nanomaterials. To further verify and understand the growth mechanism of ZnO NPs in ZnSe host, the micro-Raman scattering spectra of processed samples annealed at different temperatures were recorded (Fig. 3).

The Raman spectrum of the ZnSe annealed at 100 °C shows three major asymmetric peaks at 243, 486 and 555 cm^{-1} . The peaks at 243 and 486 cm^{-1} are assigned to the longitudinal optical phonon modes of ZnSe as 1LO and 2LO, respectively. A prominent shoulder on 243 cm^{-1} band, at 211 cm^{-1} , is also observed which is assigned to the transverse-optical (TO) phonon mode. In addition to these bands, a weak band due to the second order transverse acoustical mode (2TA) is also observed at 143 cm^{-1} . The prominent band at 555 cm^{-1} is assigned to the combination band as [2(1LO) + (TO) – 2TA]. These bands positions reasonably matched well with the previously reported data [23, 24]. We also noticed a broad background associated with bands 1LO and 2LO, which is due to the existence of amorphous ZnSe content within laser focus micro-volume. When this sample was further annealed at temperature 300 °C, a minor change in scattering intensity was noticed, however, on further annealing at 500 °C a new sharp band appears at 438 cm^{-1} with bandwidth 11 cm^{-1} . Moreover, the intensity of the other Raman bands decreases sharply. For the sample annealed at 700 °C all the bands pertaining to ZnSe disappear and only one peak at 438 cm^{-1} is visible with almost no change in bandwidth. Theoretical calculations revealed total six optical phonon branches ($A_1 + E_1 + 2B_1 + 2E_2$) in ZnO [25, 26]. Accordingly the peak at 438 cm^{-1} is assigned to E_1^{high} vibrational mode of ZnO. In addition to the peak at 438 cm^{-1} , another weak peak at 393 cm^{-1} also appears corresponding to the transition $E_1^{\text{high}} - E_2^{\text{low}}$ vibration. A rough estimation of the amount of ZnSe converted into ZnO has been made on comparing the area under the peak at 243 cm^{-1} in samples annealed at 100 and 700 °C, which was found to be reduced by more than 70 %.

3.3 Optical absorption analysis

The absorption spectra of ZnSe powder annealed at different temperatures were recorded at room temperature in the wavelength range 200–800 nm (Fig. 4). Spectra were

Table 1 Variations in miller indices (hkl), average grain size ‘D_{hkl}’ (nm), inter planner spacing ‘d’, strain ‘ε’, and lattice parameter ‘a’ & ‘c’ (Å), volume of atoms ‘V_a’, volume of cell ‘V_c’, packing fraction with annealing temperature of ZnSe

Temp (°C)	hkl	d (Å)	Strain (ε)	Average D _{hkl} (nm)	Lattice parameter	Volume of atoms (V _a)	Volume of cell (V _c)	Packing fraction (%)
100	(111)	3.258	0.440	4.2	a = 5.623	131.57	177.78	74
	(220)	1.982	0.535					
	(311)	1.694	0.589					
300	(111)	3.207	0.414	5.5	a = 5.598	129.27	174.67	74
	(220)	1.977	0.526					
	(311)	1.684	0.497					
500	(100)	2.795	0.093	18.0	a = 3.233 c = 5.157	35.38 32.94	47.81 44.45	74 74
	(002)	2.577	0.104					
	(101)	2.454	0.103					
	(102)	1.899	0.119					
	(110)	1.618	0.104					
	(103)	1.470	0.134					
	(200)	1.400	0.137					
	(112)	1.373	0.112					
	(201)	1.355	0.125					
	(202)	1.233	0.090					
700	(100)	2.785	0.060	28.0	a = 3.229 c = 5.160	35.24 33.02	47.47 44.49	74 74
	(002)	2.579	0.062					
	(101)	2.454	0.062					
	(102)	1.896	0.070					
	(110)	1.616	0.069					
	(103)	1.470	0.079					
	(200)	1.401	0.091					
	(112)	1.372	0.078					
	(201)	1.353	0.074					
	(202)	1.236	0.061					

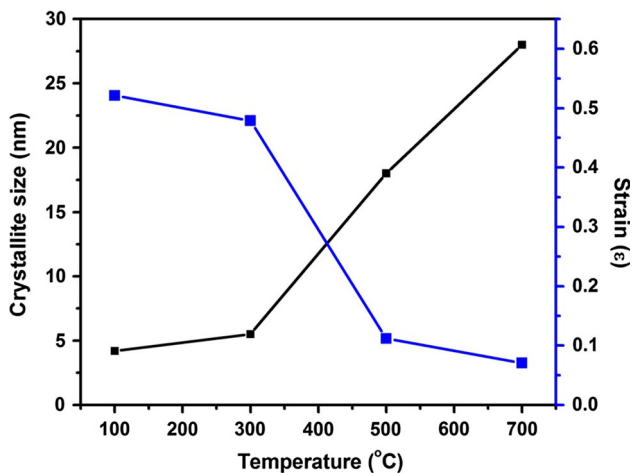


Fig. 2 Variation in crystallite size of ZnSe–ZnO sample annealed at different temperature

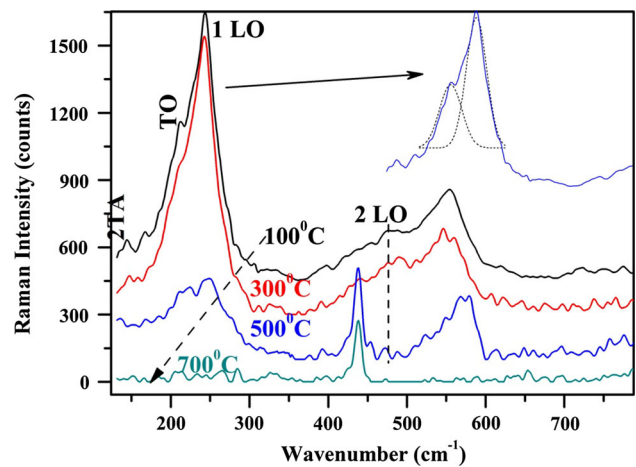


Fig. 3 Micro-Raman spectra of ZnSe–ZnO sample annealed at different temperature

monitored without taking consideration of the reflection and transmission losses.

The absorption band in the ZnSe samples, annealed at 100 and 300 °C, were found to be 415 and 384 nm, respectively while for the samples annealed at 500 and 700 °C, it is at 370 and 360 nm, respectively (Fig. 4). The blue shift is observed for ZnSe NPs as compared to the bulk ZnSe and ZnO. The reported values of band gaps are 2.7 eV (460 nm) for bulk ZnSe and 3.3 eV (375 nm) for bulk ZnO. The direct band gap, E_g , is estimated by plotting $(\alpha h\nu)^2$ versus photon energy ($h\nu$), where, α is absorption coefficient.

The value of direct band gap of the samples was determined by extrapolating the straight line portion of the graph $(\alpha h\nu)^2$ versus $h\nu$ to the $h\nu$ axis; as shown in inset of Fig. 4 and lies in the range 2.9–3.4 eV for the ZnSe–ZnO samples. The band gap of the ZnSe and the converted ZnO sample decreased with annealing temperature due to increased crystallite size.

3.4 Photoluminescence analysis

Photoluminescence spectra of synthesized ZnSe NPs at different annealing temperatures are presented in Fig. 5. When ZnSe sample, annealed at 100 °C, is excited with 370 nm the emission spectrum shows only an asymmetric peak at 470 nm corresponding to the band edge emission of ZnSe NPs. However, emission intensity of this band is reduced when sample is annealed at 300 °C.

The ZnSe sample annealed at 500 °C shows emission intensity of band edge emission reduced appreciably and a broad band centered at 590 nm (full width at half maximum 132 nm). The broad band is assigned as defect emission band of ZnO NPs due to deep-level or trap-state

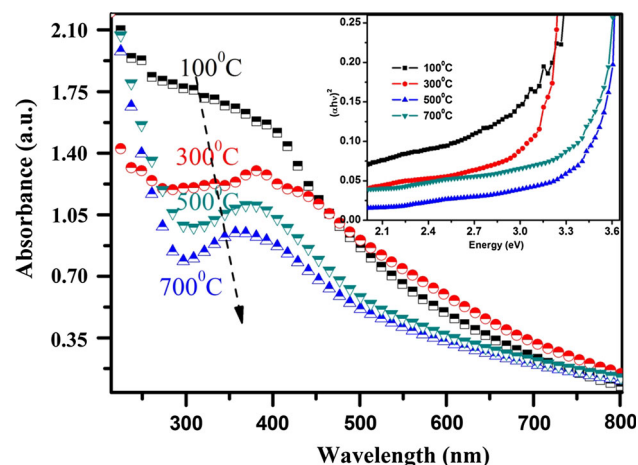


Fig. 4 Optical absorption spectra of ZnSe–ZnO sample annealed at different temperature. *Inset* $(\alpha h\nu)^2$ vs. photon energy ($h\nu$) for ZnSe–ZnO samples

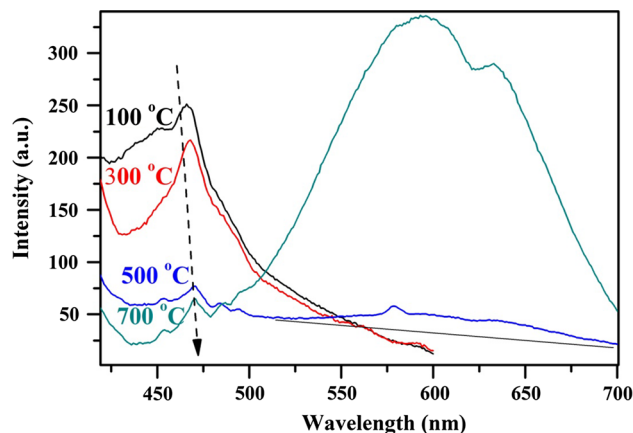


Fig. 5 Photoluminescence spectra of ZnSe samples annealed at different temperature on 370 nm excitation

emission. These trap levels are due to Zn interstitials and oxygen vacancies or related defects which are dependent on dopant concentration, nanostructures etc. In addition the ionization energies of the defects also vary from 0.05 to 2.8 eV. The intensity of broad band further increases at least three times for the sample annealed at 700 °C for 3 h, while band edge emission of ZnSe diminishes. It is evident from the emission spectrum of ZnSe (700 °C) that most of the ZnSe crystals are converted to ZnO crystals as also supported by XRD and Raman analysis.

To further verify the existence and effect of residual ZnSe NPs, we monitored the excitation spectrum of sample annealed at 700 °C, for emission at 590 nm (Fig. 6). Spectrum consists of an asymmetric broad band centered at 397 nm with a deep dip at 382 nm. Appearance of this excitation peak (at ZnSe absorption wavelength) for ZnO emission (defect emission 590 nm) is direct evidence of

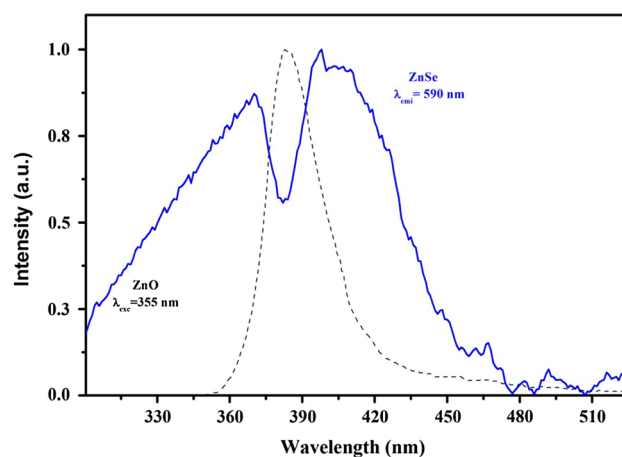


Fig. 6 Normalized excitation spectrum of ZnSe sample annealed at 700 °C for emission at 590 nm. *Dashed line* shows the emission spectrum of pure ZnO on excitation with 355 nm laser radiation

strong interaction between ZnSe and ZnO NPs through energy transfer process. A dip at 382 nm was surprising; however, it may be speculated due to the absorption by ZnO NPs through band edge. It is interesting to note that band edge emission is not visible in ZnSe sample annealed at 700 °C. It is possible that the emission due to ZnO band edge is buried in 370 nm excitation pulse. To verify the occurrence of dip due to ZnO NPs we synthesized pure ZnO NPs following the same synthesis method as for ZnSe NPs. We observed the conventional band edge emission at 382 nm (on 355 nm excitation) which is already widely reported in literature. This emission peak, at 382 nm, is well overlapped with dip in excitation spectrum of ZnSe sample annealed at 700 °C (for ZnO emission) [27, 28]. Comparing the excitation spectrum of ZnSe (700 °C) and emission spectrum of pure ZnO samples it can be concluded that some of energy in ZnSe is bypassed to defect levels of ZnO NPs through band edge levels. The possible energy transfer mechanism is expected to be through non-radiative energy transfer process.

3.5 Field emission scanning electron microscope image

Figure 7 shows FE-SEM images of the prepared samples annealed at 100 and 700 °C, respectively. It is clear that for the sample annealed at 700 °C the NPs are aggregated. Due to aggregation the size of the NPs becomes large and their shape is also not uniform. EDX spectra of the sample annealed at 100 and 700 °C are shown in Fig. 8a, b. EDX analysis confirms elemental composition of Zn and Se in the prepared sample at 100 °C with weight percentage of Zn and Se as 38.93 and 56.92 % respectively. The difference in the % composition of Zn and Se is observed even after the best experimental possible efforts as the effect of experimental error and environmental conditions cannot be completely ruled out. Therefore, a small percentage (4.15 %) of oxygen was also recorded in elemental composition analysis. The EDX spectra of the sample annealed

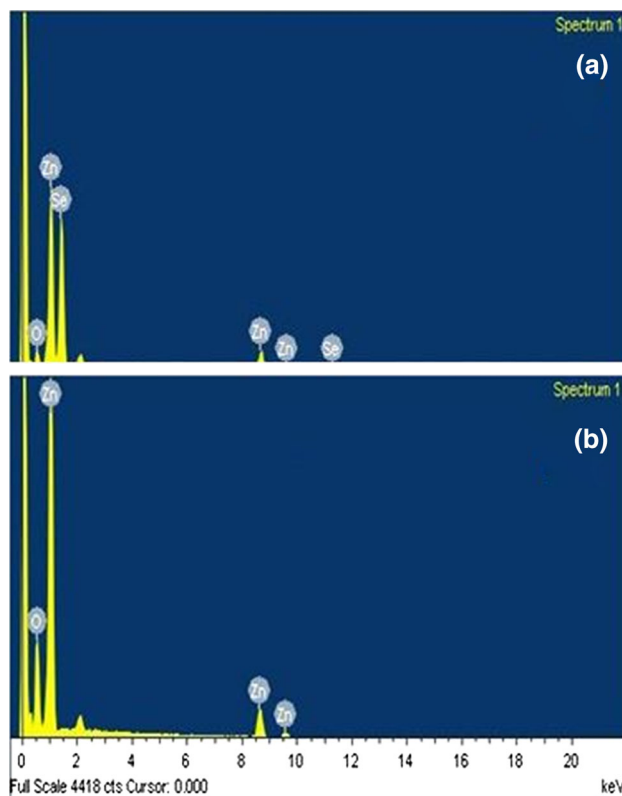


Fig. 8 EDX spectra of ZnSe–ZnO sample annealed at 100 and 700 °C temperature

at 700 °C showed absence of selenium. Quantitative analysis of the spectra showed the weight percentage of Zn and O as 45.48 and 54.52 %.

4 Conclusions

A method of systematic conversion of ZnSe NPs to ZnO NPs is reported and verified in the present studies. XRD

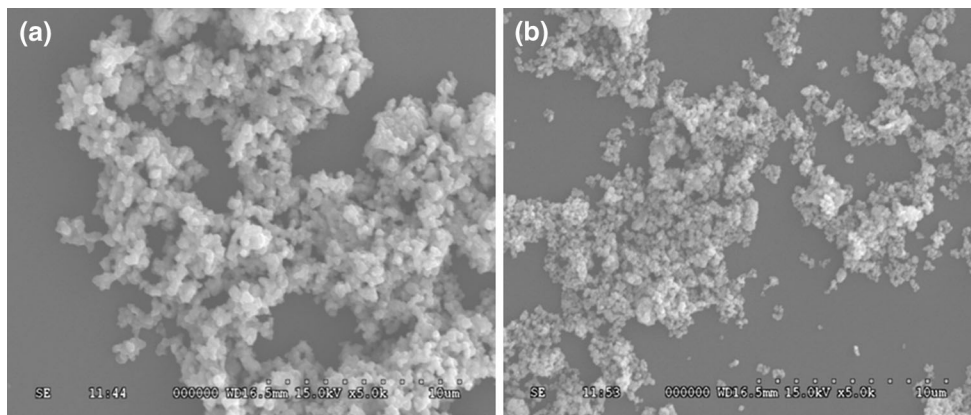


Fig. 7 FE-SEM image of ZnSe–ZnO sample annealed at 100 and 700 °C temperature

pattern revealed precipitation of cubical phase of ZnSe crystals of mean size 4.2 nm while on annealing ZnO NCs were formed of diameter 28.0 nm. Micro-Raman spectrum shows the gradual precipitation of ZnO NPs in ZnSe sample at high temperature due to oxidation process. Strong interaction between these NPs was observed in excitation spectrum which confirms the energy transfer from ZnSe NPs to ZnO NPs which yield bright emission in visible region.

Acknowledgments Authors are thankful to Dr. Inderpreet Kaur, Scientist Central Scientific Instrument Organisation, Chandigarh, Punjab for helping in recording FE-SEM and Raman spectra of the samples.

References

1. A.K. Thottoli, A.K. Achuthanunni, *J. Nano Chem.* **3**, 31 (2013)
2. S. Mathew, P.R. Rejikumar, X. Joseph, N.V. Unnikrishnan, *Opt. Mater.* **29**, 1689 (2007)
3. S. Venkatachalam, D. Mangalaraj, S.K. Narayandass, K. Kim, J. Yi, *Phys. B* **358**, 27 (2005)
4. A. Ndiaye, I. Youm, M. Cadene, *J. Sci.* **1**, 48 (2001)
5. V. Sivasubramanian, A.K. Arora, M. Premila, C.S. Sundar, V.S. Sastry, *Phys. E* **31**, 93 (2006)
6. D. Amaranatha Reddy, G. Murali, B. Poornaprakash, R.P. Vijayalakshmi, B.K. Reddy, *Solid State Commun.* **152**, 596 (2012)
7. N. Sankar, K. Ramachandran, *J. Cryst. Growth* **247**, 157 (2003)
8. Z. Lin, M. Wang, Y. Xue, X. Song, L. Zhang, X. Yao, *Ferroelectrics* **402**, 66 (2010)
9. P. Kumar, J. Singh, K. Ramam, A.C. Pandey, *J. Nanosci. Nanotech.* **13**, 377 (2013)
10. M.P. Deshpande, S.H. Chaki, N.H. Patel, S.V. Bhatt, B.H. Soni, *J. Nano Electron. Phys.* **3**, 193 (2012)
11. P.V. Kamat, *J. Phys. Chem. C* **112**, 18737 (2008)
12. L. Peng, Y. Wang, Q. Dong, Z. Wang, *Nano-Micro Lett.* **2**, 190 (2010)
13. J. Lim, S. Jun, E. Jang, H. Baik, H. Kim, J. Cho, *Adv. Mater.* **19**, 1927 (2007)
14. K.R. Murali, A. Austine, D.C. Trivedi, *Mater. Lett.* **59**, 2621 (2005)
15. H. Wang, F. Du, *Cryst. Res. Technol.* **41**, 23 (2006)
16. R. John, S.S. Florence, *Chalcogenide Lett.* **7**, 269 (2010)
17. J.P. Borah, J. Barman, K.C. Sharma, *Chalcogenide Lett.* **5**, 201 (2008)
18. G. Ghosh, M.K. Naskar, A. Patra, M. Chatterjee, *J. Opt. Mater.* **28**, 1047 (2006)
19. R. Tamrakar, M. Ramrakhiani, B.P. Chandra, *Open Nano Sci.* **2**, 12 (2008)
20. L.S. Wang, R.Y. Hong, B. Reddy (eds.), *Advances in Nanocomposites—Synthesis, Characterization and Industrial Applications* (InTech Publications, India, 2011)
21. G. Skandan, A. Singhal, C.I. Contescu, K. Putyera (eds.), *Dekker Encyclopedia of Nanoscience and Nanotechnology* (Taylor and Francis Group, New York, 2009), p. 2788
22. S.S. Kale, C.D. Lokhande, *Mater. Chem. Phys.* **62**, 103 (2000)
23. J. Xu, X. Yang, Q.D. Yang, T.L. Wong, S.T. Lee, W.J. Zhang, C.S. Lee, *J. Mater. Chem.* **22**, 13374 (2012)
24. G. Lu, H. An, Y. Chen, J. Huang, H. Zhang, B. Xiang, Q. Zhao, D. Yu, W. Du, *J. Cryst. Growth* **274**, 530 (2005)
25. S. Sahoo, S.K. Barik, A.P.S. Gaur, M. Correa, G. Singh, R.K. Katiyar, V.S. Puli, J. Liriano, R.S. Katiyar, *J. Solid State Sci. Tech.* **1**, 140 (2012)
26. R. Seth, K.L. Gosain, N. Jaggi, S. Panwar, S. Kumar, *Nonlinear Opt. Quantum Opt* **44**, 259 (2012)
27. I. Shalish, H. Temkin, V. Narayanamurti, *Phys. Rev. B* **69**, 245401 (2004)
28. Y. Dwivedi, *J. Nanoeng. Nanomanuf.* **3**, 337 (2013)